Supporting Information

Sample Preparation. All protein samples were expressed in *E.* coli BL21 DE3 bacteria harboring the G48M expression plasmid (*1, 2*). Cultures were grown on 99% $^{2}H_2O$ M9 media with $^{15}NH_4Cl$ and U-^{2}H,^{12}C glucose as the sole sources of nitrogen and carbon. For one of the samples, 85 mg/L α-ketoisovalerate ($^{12}COO^{-}$-^{12}CO-$^{12}C^{2}H$-[$^{13}C^{1}H_3$]$_2$), 50 mg/L α-ketobutyrate ($^{12}COO^{-}$-^{12}CO-$^{12}C^{2}H_2$-$^{13}C^{1}H_3$) (Isotec), and 75 mg/L U-^{1}H,^{12}C,$^{2}H^{\alpha}$ phenylalanine and tryptophan were added 1 hour prior to the induction of expression, as described previously (*3, 4*). Substitution of protium with deuterium at the H^{α} positions of phenylalanine and tryptophan was achieved by incubating the amino acids in 99% $^{2}H_2O$, 50 mM $K_2{}^{2}HPO_4$ at pH^{*} 6.6 with a broad-spectrum transaminase (Sigma) and 0.2 mM pyridoxal-5-phosphate at 37°C overnight. Both protein samples were purified by liquid chromatography as described elsewhere (*2*).

NMR Experiments. ^{15}N single-quantum (*5, 6*), ^{1}H single-quantum (*7*), $^{15}N/^{1}H$ double-quantum and zero-quantum (*8*), and $^{15}N/^{1}H$ multiple quantum (*9*) relaxation dispersion experiments were performed on the perdeuterated protein sample at 25°C using Varian INOVA spectrometers operating at 500, 600, and 800 MHz proton frequencies. For the selectively ^{1}H,^{13}C-labeled sample, ^{15}N and ^{1}H single-quantum (20°C:500,800 MHz; 25°C:500,600,800 MHz; 30°C:500,800 MHz), $^{15}N/^{1}H$ double- and zero-quantum (20°C:500,800 MHz; 25°C:600,800 MHz; 30°C:500 MHz), and $^{15}N/^{1}H$ multiple quantum (20°C:500,800 MHz; 25°C:600,800 MHz; 30°C:500,800 MHz) experiments were performed. In addition, ^{13}C single-quantum dispersion pulse schemes (*10*) were employed for this sample at 20°C, 25°C and 30°C using 500 MHz and 800 MHz spectrometers.

Dispersion Profiles. Effective transverse relaxation rates, $R_{2,eff}$, were calculated from the ratio of peak intensities in spectra with (I) and without (I_0) relaxation delays of length T, according to $R_{2,eff}=-ln[I/I_0]/T$. T values of (40ms, 40ms, 30ms) for ^{15}N single-quantum, (30ms, 30ms, 20ms) for ^{1}H single-quantum, (40ms, 40ms, 30ms) for ^{13}C single-quantum, (30ms, 30ms, 20ms) for $^{15}N/^{1}H$ double/zero-quantum, and (20ms, 20ms, 20ms) for $^{15}N/^{1}H$ multiple-quantum experiments were employed at (20°C, 25°C, 30°C). The relative error, $\sigma_{R2eff}/R_{2,eff}$, was assumed to be the same for all points in a dispersion profile and was calculated from repeat experiments as

$$\sigma_{R2eff}/R_{2,eff} = (\Sigma(\Delta R_i)^2/(n-1))^{0.5}, \quad \text{(S1)}$$

where the sum extends over all (n) duplicated $R_{2,eff}$ points,

$$\Delta R_i = (R_{2,eff,i}(\nu) - \langle R_{2,eff}(\nu)\rangle)/\langle R_{2,eff}(\nu)\rangle, \quad \text{(S2)}$$

$R_{2,eff,i}(\nu)$ is a single $R_{2,eff}$ measurement at $\nu_{CPMG} = \nu$, and $\langle\rangle$ indicates averaging over all duplicate $R_{2,eff}$ measurements in the profile with $\nu_{CPMG} = \nu$. Relative errors below threshold values of (2%, 2%, 2%) for ^{15}N and ^{1}H single-quantum, (3%, 3%, 4%) for ^{13}C single-quantum, (5%, 5%, 5%) for $^{15}N/^{1}H$ double/zero-quantum, and (2%, 2%, 5%) for

$^{15}N/^{1}H$ multiple-quantum experiments at (20°C, 25°C, 30°C) were readjusted to the threshold values.

Data were fit together using in-house software, employing both two-site (Unfolded ⇔ Folded) and three-site (Unfolded ⇔ Intermediate ⇔ Folded) models of exchange. In the case of single-quantum experiments and two-site exchange, $R_{2,eff}=f[\nu_{CPMG},k_{UF},k_{FU},\Delta\omega_{FU},R_{2,eff}(\infty)]$, and for three-site exchange, $R_{2,eff}=f[\nu_{CPMG},k_{UI},k_{IU},k_{IF},k_{FI},\Delta\omega_{FU},\Delta\omega_{FI},R_{2,eff}(\infty)]$, where k_{XY} is the first order rate constant for conversion from state X to state Y, $\Delta\omega_{XY}$ is the difference in ^{1}H or ^{15}N chemical shifts between states X and Y, $R_{2,eff}(\infty)$ is the theoretical transverse relaxation rate for $\nu_{CPMG}=\infty$, and *f* is a complicated function that varies with the dynamic model and is calculated numerically (*8, 9, 11*). $R_{2,eff}$ depends on both ^{1}H and ^{15}N chemical shift differences in the case of double, zero, and multiple quantum experiments.

Backbone Data. Initially, data at 20°C, 25°C, 30°C were fit separately. At 20°C and 25°C, 47 well-resolved amide peaks showed measurable broadening and were used in the analyses. At 30°C, 43 residues were used in the calculations. For each temperature, the following protocol was employed:

1) Two-site exchange models (U⇔F) were fit on a per-residue basis, employing ^{15}N and ^{1}H single quantum data. Multiple-, double-, and zero-quantum $^{15}N/^{1}H$ data were then included in the fits, establishing the relative signs of ^{15}N and ^{1}H chemical shift differences, $\Delta\omega_{FU}$. In what follows, amide single-, multiple-, double-, and zero-quantum data were included.
2) A four-dimensional grid search was performed for each residue, varying the global parameters of a three-site exchange model (U⇔I⇔F). The populations of I and U states were fixed such that $p_I, p_U \in \{.001, .005, .01, .02, .03, .04, .05, .06, .07, .08, .09\}$, $p_I+p_U < .1$. The U,I and I,F exchange rates were fixed such that $k_{UI}+k_{IU}$, $k_{IF}+k_{FI} \in \{158, 251, 398, 631, 1000, 1585, 2512, 3981, 6310, 10000, 15849\}$. For each of the 9196 iterations (i.e., 9196 grid points), χ^2 minimizations were performed holding the global exchange parameters fixed, and optimizing $\Delta\omega_{FU}(^{15}N)$, $\Delta\omega_{FU}(^{1}H)$, $\Delta\omega_{FI}(^{15}N)$, $\Delta\omega_{FI}(^{1}H)$ and $R_{2,eff}(\nu_{CPMG}=\infty)$ values. Initial values of $\Delta\omega_{FU}$ were set to the results obtained in step 1). Two minimizations were performed per iteration, with starting conditions of $\Delta\omega_{FI}=\Delta\omega_{FU}$ and $\Delta\omega_{FI}=0$, with the better of the two solutions being retained.
3) The twenty grid-search iterations giving the overall lowest χ^2 values, summing over all residues, were used to initialize minimizations in which data for all (47 or 43) residues were fit together, and global exchange parameters were optimized along with $\Delta\omega$ and $R_{2,eff}(\infty)$ values.
4) During the course of optimization, χ^2 values were periodically tested for false minima by fixing global parameters and reinitiating calculations from a grid of different $\Delta\omega$ values. Specifically, for each set of $\{\Delta\omega_{FU}(^{15}N), \Delta\omega_{FU}(^{1}H), \Delta\omega_{FI}(^{15}N), \Delta\omega_{FI}(^{1}H)\}$ that are obtained on a per-residue basis, minimizations are started from 7 other points corresponding

to other signed combinations of the chemical shifts above, i.e., $\{\Delta\omega_{FU}(^{15}N), \pm\Delta\omega_{FU}(^{1}H), \pm\Delta\omega_{FI}(^{15}N), \pm\Delta\omega_{FI}(^{1}H)\}$.

5) In the first several rounds of minimization, this procedure would typically improve the fits of 5 to 10 residues. In later rounds, all residues were found to have optimal $\Delta\omega$ values, without the need for this adjustment. Overall, 200, 200 and 60 steps of minimization were employed for data at 20°C, 25°C and 30°C, respectively.

6) The signs of chemical shift differences were obtained using an extension of the approach of Skrynnikov et al. (*12*) that will be described in detail elsewhere.

A final minimization was performed, combining 20°C, 25°C and 30°C data for 42 residues (2, 3, 5, 7, 9, 10, 11, 12, 13, 15, 17, 19, 20, 21, 22, 23, 24, 26, 27, 28, 29, 30, 33, 34, 35, 38, 39, 40, 41, 49, 43, 44, 46, 47, 48, 50, 52, 54, 55, 56, 58, 59), assuming that values of $\Delta\omega$ are temperature-independent. Independent exchange parameters (k_{UI}, k_{IU}, k_{IF}, k_{FI}) were obtained for each temperature. The calculations proceeded as follows:

1) $\Delta\omega$ parameters from the ten best global minimizations at each temperature were combined, such that each of $\Delta\omega_{FU}(^{15}N)$, $\Delta\omega_{FU}(^{1}H)$, $\Delta\omega_{FI}(^{15}N)$, and $\Delta\omega_{FI}(^{1}H)$ had a set of thirty estimates for each residue.

2) For each $\Delta\omega$ set (of which there are 30), a randomized bootstrap sample (*13*) was drawn and the median calculated. This was repeated ten times, and the median $\Delta\omega$ values were used to initialize ten minimizations.

3) For each of the ten minimizations, $\Delta\omega$ values were held fixed to their bootstrap median values while global exchange parameters were optimized. Subsequently, both global exchange parameters and $\Delta\omega$ values were fit simultaneously.

4) χ^2 values were periodically tested for false minima, as described above. Each of the ten calculations underwent 240 steps of minimization. Reported values (uncertainties) in Table S1 are the means (standard deviations) of the ten solutions.

Note that chemical shift differences between F, I and U states for Val 55 were so great that they were difficult to determine with accuracy, and these values were not included in Figure 2 or in other comparisons.

Table S1. Global Exchange parameters for selectively-protonated G48M

Temperature	k_{UI} s^{-1}	k_{IU} s^{-1}	k_{IF} s^{-1}	k_{FI} s^{-1}	ΔG_{UI} kcal/mole	ΔG_{UF} kcal/mole
20°C	1300±100	6000±200	2000±200	13±1	0.89±0.05	-2.10±0.01
25°C	1700±200	8000±200	3000±400	22±1	0.91±0.06	-1.99±0.01
30°C	1800±200	9000±300	4000±500	41±1	0.98±0.06	-1.81±0.01

Side-Chain Data. All well-resolved ^{13}C-labeled methyl peaks (Leu, Ile δ; Val γ) of G48M exhibit sizable exchange contributions to relaxation. Three methyl-containing residues in the amino- and carboxy- terminal linker regions, beyond the sequence of the domain, do not show broadening. The two methyl peaks of Val 58 are overlapped and were not included in the analysis, leaving 14 methyl groups (L3δ1, L3δ2, L7δ1, L7δ2, L18δ1, L18δ2, I28δ1, L29δ1, L29δ2, L42δ1, L42δ2, I50δ1, V55γ1, V55γ2) in the calculations. Data at 20°C, 25°C, and 30°C were fit together on a per-methyl basis, holding global exchange parameters fixed to the values obtained from backbone measurements and assuming that methyl Δω values are temperature-independent. A representative fit is shown in Fig. S1. This was repeated for each of the ten backbone solutions and reported Δω values (uncertainties) are the means (standard deviations) of values extracted from the ten computations.

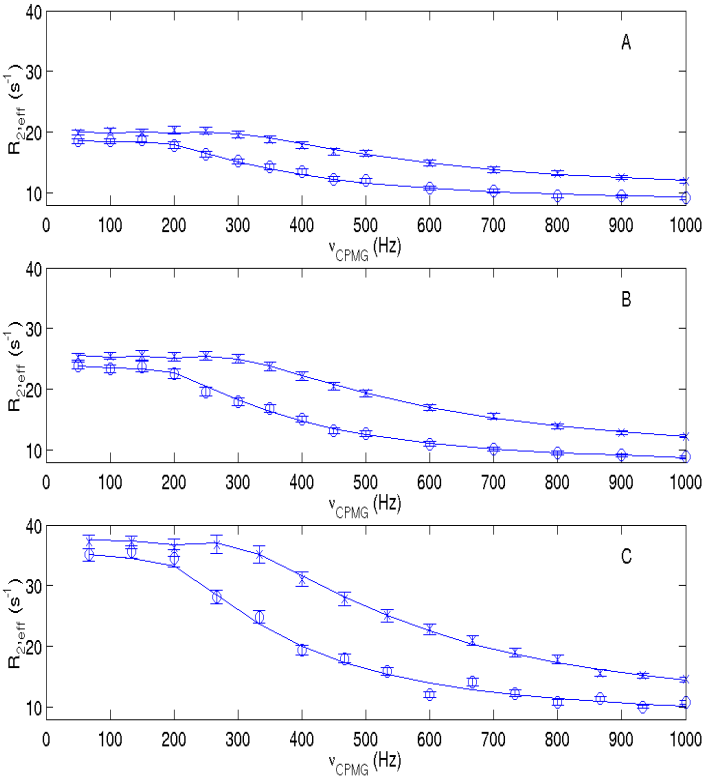

Figure S1. Fits of 20°C (A), 25°C (B), and 30°C (C) ^{13}C single-quantum dispersion data for the δ1 methyl group of Ile 28 in G48M. $R_{2,eff}$ values obtained at 500 MHz (o) and 800 MHz (x) (^{1}H Larmor frequencies) are plotted together with solid lines representing best-fit values. Fits were calculated with backbone-derived global exchange parameters (first of ten solutions, k_{UI}=1345, 1767, 1838 s^{-1}, k_{IU}=6040, 8205, 9331 s^{-1}, k_{IF}=2176, 2930, 4120 s^{-1}, k_{FI}=13.2, 21.9, 40.2 s^{-1} at 20°C, 25°C, 30°C, respectively) and with the assumption that ^{13}C $\Delta\omega_{FU}$ and $\Delta\omega_{FI}$ values are temperature independent.

Two versus Three Site Models. ^{15}N, ^{1}H, and ^{13}C single-quantum data were used to compare two site (U⇔F) and three-site (U⇔I⇔F) models of exchange. Only single quantum dispersion data sets were selected, recorded at a pair of external magnetic fields, so that effectively the same amount of data was compared for each nucleus type. Data obtained at 500 MHz and 800 MHz spectrometer frequencies were used for all nuclei at 20°C and 30°C. In the case of ^{15}N and ^{1}H nuclei at 25°C, 600 MHz and 800 MHz data were employed, while for ^{13}C nuclei at 25°C, 500 MHz and 800 MHz data were used. Each minimization employed only measurements for a single nucleus type. For both two-site and three-site models, data at all temperatures were fit together, assuming that $\Delta\omega$ values do not vary with temperature, and optimizing global exchange parameters independently at each temperature. The initial global exchange parameters for all two-site minimizations were p_U=.032, .040, .056 and $k_{UF}+k_{FU}$=3000, 4000, 5000 s^{-1} at 20°C,

25°C, 30°C. The initial parameters for all three-site minimizations were taken from a separate calculation in which ^{15}N, ^{1}H, and ^{13}C data were fit simultaneously.

References

1. **Di Nardo, A. A., Korzhnev, D. M., Stogios, P. J., Zarrine-Afsar, A., Kay, L. E., and Davidson, A. R. (2004) Dramatic acceleration of protein folding by stabilization of a nonnative backbone conformation, *Proceedings of the National Academy of Sciences of the United States of America 101*, 7954-7959.**
2. **Maxwell, K. L., and Davidson, A. R. (1998) Mutagenesis of a buried polar interaction in an SH3 domain: sequence conservation provides the best prediction of stability effects, *Biochemistry 37*, 16172-16182.**
3. **Goto, N. K., Gardner, K. H., Mueller, G. A., Willis, R. C., and Kay, L. E. (1999) A robust and cost-effective method for the production of Val, Leu, Ile (δ1) methyl-protonated ^{15}N-,^{13}C-,^{2}H-labeled proteins, *J. Biomol. NMR 13*, 369-374.**
4. **Crowhurst, K. A., and Forman-Kay, J. D. (2003) Aromatic and methyl NOEs highlight hydrophobic clustering in the unfolded state of an SH3 domain, *Biochemistry 42*, 8687-8695.**
5. **Mulder, F. A. A., Mittermaier, A., Hon, B., Dahlquist, F. W., and Kay, L. E. (2001) Studying excited states of proteins by NMR spectroscopy, *Nat. Struct. Biol. 8*, 932-935.**
6. **Tollinger, M., Skrynnikov, N. R., Mulder, F. A., Forman-Kay, J. D., and Kay, L. E. (2001) Slow dynamics in folded and unfolded states of an SH3 domain, *J. Am. Chem. Soc 123*, 11341-11352.**
7. **Ishima, R., and Torchia, D. A. (2003) Extending the range of amide proton relaxation dispersion experiments in proteins using a constant-time relaxation-compensated CPMG approach, *Journal of Biomolecular Nmr 25*, 243-248.**
8. **Orekhov, V. Y., Korzhnev, D. M., and Kay, L. E. (2004) Double- and zero-quantum NMR relaxation dispersion experiments sampling millisecond time scale dynamics in proteins, *Journal of the American Chemical Society 126*, 1886-1891.**
9. **Korzhnev, D. M., Kloiber, K., and Kay, L. E. (2004) Multiple-quantum relaxation dispersion NMR spectroscopy probing millisecond time-scale dynamics in proteins: Theory and application, *Journal of the American Chemical Society 126*, 7320-7329.**
10. **Skrynnikov, N. R., Mulder, F. A. A., Hon, B., Dahlquist, F. W., and Kay, L. E. (2001) Probing slow time scale dynamics at methyl-containing side chains in proteins by relaxation dispersion NMR measurements: Application to methionine residues in a cavity mutant of T4 lysozyme, *J. Am. Chem. Soc. 123*, 4556-4566.**
11. **Korzhnev, D. M., Salvatella, X., Vendruscolo, M., Di Nardo, A. A., Davidson, A. R., Dobson, C. M., and Kay, L. E. (2004) Low-populated folding**

intermediates of Fyn SH3 characterized by relaxation dispersion NMR, ***Nature 430*****, 586-590.**

12. **Skrynnikov, N. R., Dahlquist, F. W., and Kay, L. E. (2002) Reconstructing NMR spectra of "invisible" excited protein states using HSQC and HMQC experiments,** ***Journal of the American Chemical Society 124*****, 12352-12360.**
13. **Efron, B., and Tibshirani, R. (1986) Bootstrap methods for standard errors, confidence intervals and other measures of statistical accuracy,** ***Stat. Sci. 1*****, 54-77.**